Mineralogical Magazine, October 2011, Vol. 75(5), pp. 2631–2648

Galuskinite, $Ca_7(SiO_4)_3(CO_3)$, a new skarn mineral from the Birkhin gabbro massif, Eastern Siberia, Russia

B. Lazic[1], T. Armbruster[1,*], V. B. Savelyeva[2], A. E. Zadov[3], N. N. Pertsev[4] and P. Dzierżanowski[5]

[1] Institute of Geological Sciences, University of Bern, Freiestr. 3, CH-3012 Bern, Switzerland
[2] Institute of the Earth Crust SB RAS, Lermontov St. 128, 664033 Irkutsk, Russia
[3] OOO Science Research Centre 'NEOCHEM', Altuf'evskoye Highway 43, Moscow, Russia
[4] Institute of Geology of Ore Deposits, Petrography, Mineralogy and Geochemistry (IGEM) RAS, Staromonetny 35, Moscow, Russia
[5] Institute of Geochemistry, Mineralogy and Petrology, University of Warsaw, al. Żwirki i Wigury 93, 02-089 Warszawa, Poland

[*Received 2 March 2011; Accepted 12 July 2011*]

ABSTRACT

In addition to spurrite, $Ca_5(SiO_4)_2(CO_3)$, and tilleyite, $Ca_5(Si_2O_7)(CO_3)_2$, galuskinite, $Ca_7(SiO_4)_3(CO_3)$, is the third mineral in the $CaO-SiO_2-CO_2$ ternary system. Galuskinite, monoclinic, space group $P2_1/c$ (a = 18.79, b = 6.72, c = 10.47 Å, β = 90.79º, V = 1322 Å^3, Z = 4), occurs in thin veins which cut calcio-olivine, γ-Ca_2SiO_4, skarn with larnite, β-Ca_2SiO_4, relics. Pavlovskyite, $Ca_8(SiO_4)_2(Si_3O_{10})$, and dellaite, $Ca_6(Si_2O_7)(SiO_4)(OH)_2$, form a margin between the veins and the calcio-olivine skarn. The sanidinite facies high-temperature skarn formed ~500 Ma ago when gabbroid rocks of the Birkhin complex (Baikal area, Eastern Siberia, Russia) intruded and contact-metamorphosed limestone xenoliths. Galuskinite is a retrograde product of skarn alteration and has neither been described from cement clinker production processes nor from studies of the $CaO-SiO_2-CO_2$ system. The crystal structure of galuskinite, refined from single crystal X-ray data to R_1 = 3.1%, has a modular character. One may define a polysomatic series with spurrite and larnite as endmembers and galuskinite as a 1:1 polysome built from regular alternating spurrite and larnite modules. Differences between the X-ray powder patterns of galuskinite and spurrite are most obvious in the low θ region. Galuskinite is named after the Russian mineralogists Irina O. Galuskina and Evgeny V. Galuskin, Faculty of Earth Sciences, University of Silesia, Poland, for their outstanding contributions to skarn mineralogy.

Keywords: galuskinite, calcium silicate carbonate, skarn, new mineral, crystal structure, polysomatism, modularity, Baikal, Russia.

Introduction

The crystalline phases in the $CaO-SiO_2-CO_2$ system (Eitel, 1923; Wyllie and Haas, 1965, 1966; Zharikov and Shmulovich, 1969; Treiman and Essene, 1983) are commonly associated either with cement production or are found as products of contact metamorphism and metasomatism of limestone (Treiman and Essene, 1983). Two minerals have been reported previously in this ternary system: spurrite, $Ca_5(SiO_4)_2(CO_3)$ and tilleyite, $Ca_5(Si_2O_7)(CO_3)_2$ and both have been structurally reinvestigated and compared with other silicate carbonate minerals recently (Grice, 2005). Spurrite is an orthosilicate whereas tilleyite is a disilicate. Silicate and carbonate groups occupy separate layers in these minerals because their Lewis-base strength is quite different: "...[SiO_4] has 0.33 valence units (*vu*), and [Si_2O_7] has 0.30 *vu*), whereas the [CO_3] group

* E-mail: thomas.ambruster@krist.unibe.ch
DOI: 10.1180/minmag.2011.075.5.2631

has 0.22 *vu*. The silicate group occupies the layer with cationic groups of higher Lewis-acid strength, and the carbonate group occupies the layer with cationic groups of lower Lewis-acid strength" (Grice, 2005). Further insight into this valence-matching principle is provided by Hawthorne and Schindler (2008).

If H_2O is included as an additional component (i.e. in the system $CaO-SiO_2-CO_2-H_2O$) the minerals fukalite, $Ca_4Si_2O_6(OH)_2(CO_3)$ (Henmi *et al*., 1977; Merlino *et al*., 2009) and scawtite, $Ca_7(Si_6O_{18})(CO_3)\cdot 2H_2O$ (Tilley and Hey, 1930; Grice, 2005), are known. Ignoring minor Cl^- concentrations, defernite, $Ca_6(CO_3)_{1.58}(Si_2O_7)_{0.21}(OH)_7[Cl_{0.5}(OH)_{0.08}(H_2O)_{0.42}]$ (Sarp *et al*., 1980; Armbruster *et al*., 1996), could also be considered as part of the system. Fukalite has an OD structure with two-dimensional disorder. Its modular structure consists of tobermorite-like Ca polyhedral layers alternating along *b* with tilleyite-type zigzag polyhedral layers; silicate chains with a periodicity of four tetrahedra run along *a*; and the CO_3 groups are linked to the gaps of the tobermorite layer and alternate with silicate chains (Merlino *et al*., 2009). Scawtite has a layer structure parallel to (101) which is composed of a $[CaO_{6-8}]$ polyhedral sheet linked by Si_6O_{18} rings and isolated CO_3 groups (Grice, 2005). Defernite is characterized by a microporous framework formed by edge- and corner-sharing CaO_{6-7} polyhedra, which are also linked by CO_3 groups aligned parallel to the (001) plane. Its framework has channels parallel to the *c* axis, which are confined by eight-membered rings of CaO_{6-7} polyhedra and the Si_2O_7 units randomly substitute for two stacked CO_3 triangles (Armbruster *et al*., 1996).

Spurrite is formed during the cement producing process, in the presence of CO_2 in the kiln atmosphere, when clinker is heated to 750–900ºC. Fluoride, chloride and K_2O seem to favour spurrite formation (Glasser, 1973; Bolio-Arceo and Glasser, 1990; Taylor, 1997). Tuttle and Harker (1957) studied the reaction wollastonite + calcite → spurrite + CO_2. The temperature of spurrite formation increases with CO_2 pressure, reaching 1000ºC at 345 bar. Spurrite and tilleyite have also been synthesized hydrothermally using oxalic acid as a CO_2 source at 1 kbar at 430 and 450ºC, respectively (Henmi and Henmi, 1978). However, tilleyite has not been found as a product during the manufacture of clinker (Taylor, 1997). Among the hydrous calcium silicate carbonates only scawtite has been synthesized. The synthesis of scawtite was successful at low partial pressures of CO_2, with H_2O in excess. Scawtite is formed at temperatures between 140ºC and 300ºC (e.g. Kapralik *et al*., 1984; Garbev, 2004).

Spurrite is found characteristically in high-temperature skarns formed during the shallow intrusion of igneous rock into limestone (Wright, 1908; Tilley, 1929; Joesten, 1976; Galuskin *et al*., 2009; Galuskina *et al*., 2009). It also occurs in the pyrometamorphic rocks of the Hatrurim Formation in Israel (Sokol *et al*., 2008) where the combustion of organic fossil fuel provides a heat source. The conditions of formation for spurrite and tilleyite are similar and the minerals are occasionally found in association with each other (Marincea *et al*., 2001; Beard and Drake, 2007).

The discovery of the new skarn mineral galuskinite, $Ca_7(SiO_4)_3(CO_3)$, in the well known system $CaO-SiO_2-CO_2$ (Wyllie and Haas, 1966; Zharikov and Shmulovich, 1969) is surprising. A synthetic analogue of galuskinite has neither been found in the process of cement production nor produced experimentally. This study reports the occurrence, properties and crystal structure of this unusual mineral.

In February 2011, the IMA-CNMNC approved mineral proposal no. 2010-057 and the mineral name galuskinite. Galuskinite is named in honour of the Russian mineralogists Irina Olegovna Galuskina (born 1961) and Evgeny Vadimovich Galuskin (born 1960), who work at the Faculty of Earth Sciences, University of Silesia, Poland. Both have discovered and described more than fifteen new minerals from high-temperature skarns in Russia (northern Caucasus, Baikal region, Sakha-Yakutia). Their studies have had an important impact on our understanding of high-temperature skarn mineralogy and on economic mineralogy as artificial analogues of several of the new minerals occur as mainly microcrystalline phases in cement and clinker. Holotype samples of galuskinite are deposited in the collections of the A.E. Fersman Mineralogical Museum of the Russian Academy of Sciences, catalogue number 4050/1 and in the collections of the Natural History Museum, Bern, catalogue number NMBE-40811.

Geological setting of galuskinite occurrence

The Birkhin gabbroid massif is situated in the Olkhon region of Eastern Siberia, which includes the west coast of the Lake Baikal and Olkhon

Island (Fig. 1*a*). It is interpreted as fragment of a collisional system formed in the Early Palaeozoic when a number of terranes accreted onto the margins of the Siberian Craton (Donskaya *et al*., 2000). The structure of the Olkhon region is considered as a stack of shear slabs (Fig. 1*a*) which are composed of metamorphic and magmatic rocks (Fedorovsky and Sklyarov, 2010; Fedorovsky *et al*., 2010). The metamorphic grade increases from southeast to west and northwest from epidote-amphibolite to granulitic facies.

The Birkhin massif has an isometric shape and is 13 km in diameter (Fig. 1*b*). Geophysical data show that it has a lopolith- or harpolith-like form (Novoselova and Turutanov, 1982). The massif is a part of the homonymous sub-alkaline complex of monzogabbro and monzodiorite and was formed by two intrusive phases. The first intrusive component at the central part of the massif consists of low-alkaline gabbroid rocks (differentiated pyroxenite–gabbro-norite–anorthosite series). The second component, which accounts for more than 70% of the massif, consists of monzogabbroid and differentiated rock series with compositions ranging from olivine gabbro-norite to monzodiorite (Mekhonoshin *et al*., 2004). The age of the monzogabbro is 499 Ma (Fedorovsky and Sklyarov, 2010; Fedorovsky *et al*., 2010).

The Birkhin gabbroid massif is surrounded by marble, amphibolite, garnet-biotite gneiss and other metamorphic rocks. The contacts between it and the surrounding rocks are mainly tectonic. Fragments of amphibolite hornfels are found at the south and southeast contact. Rocks at the southeast contact of the massif are metamorphosed up to the staurolite-chlorite-andalusite grade (T = 480–500ºC, P = 3.5 kbar) (Korikovsky and Fedorovsky, 1981). At the contact with gabbroid rocks, metamorphism has produced a two-pyroxene hornfels facies. Vladimirov *et al*. (2009) proposed the following model of massif formation. In the early stages, ~500 Ma, intrusion of the gabbroid rocks of the Birkhin complex into the metamorphic country rocks led to the formation of hornfelsed zones at the contacts (and probably, high-temperature skarns were produced). During the period from 480–465 Ma, at the peak of collision events, the gabbroid body was exhumed to the upper levels of earth crust. During the later stage, 440–410 Ma, post collision events, the Birkhin massif became a consolidated body and the enclosing rocks underwent mylonitization as a result of brittle and viscoplastic deformation produced by left-lateral tectonic movement along the Siberian Plate.

Galuskinite was found in altered silicate-carbonate xenoliths a few metres in diameter in the Birkhin gabbro massif (52.7ºN 106.5ºE). The skarns of the Birkhin gabbroid massif are famous for large kilchoanite, $Ca_6(SiO_4)(Si_3O_{10})$, aggregates (Savelyeva *et al*., 1992). Galuskinite is associated with pavlovskyite (IMA2010-63), another recently discovered mineral (Galuskin *et al*., 2011).

Further minerals noted from the Birkhin skarns include calcio-olivine, larnite, bredigite, merwinite, monticellite, spinel, magnetite, members of the gehlenite–åkermanite series, garnet of the grossular–andradite–schorlomite–kerimasite series, kilchoanite, pavlovskyite, cuspidine, baghdadite, chlorbartonite, pyrrhotite, hydroxylellestadite, spurrite, clintonite, fluorapatite and hydroxylapatite, hillebrandite, perovskite, wollastonite, dellaite and vesuvianite.

Galuskinite occurs in thin veins cutting calcio-olivine skarn with relict larnite, in which sporadic grains of bredigite, $Ca_7Mg(SiO_4)_4$, gehlenite, $Ca_2Al_2SiO_7$, cuspidine, $Ca_4Si_2O_7F_2$ and hydroxylellestadite, $Ca_{10}(SiO_4)_3(SO_4)_3(OH,F)_2$, are present (Fig. 2). The central part of the veins are composed of galuskinite. Pavlovskyite and dellaite form a margin between the core and the calcio-olivine skarn (Fig. 3*a*–*e*). Galuskinite grains up to 0.5 mm in size are heavily fractured and twinned (Fig. 3*f*); both simple and polysynthetic twins are noted.

Experimental methods

Sixty point-analyses were carried out using a CAMECA SX100 electron microprobe operating in wavelength-dispersive mode at 15 kV, 10–20 nA, with a ~1 μm beam diameter. Natural and synthetic standards were employed. The following lines and standards were used for the galuskinite analyses: Ca-*K*α, Si-*K*α, wollastonite; P-*K*α, apatite; Na-*K*α, albite; S-*K*α, baryte.

Raman spectra of single crystals of galuskinite (Fig. 4) were recorded using a Dilor XY spectrometer equipped with a 1800 line mm^{-1} grating monochromator, a charge-coupled device (CCD), Peltier-cooled detector (1024×256) and an Olympus BX40 confocal microscope. The incident laser excitation was provided by a water-cooled argon laser source operating at 514.5 nm. The power at the exit of a 100× objective lens varied from 30–50 mW. Raman spectra were

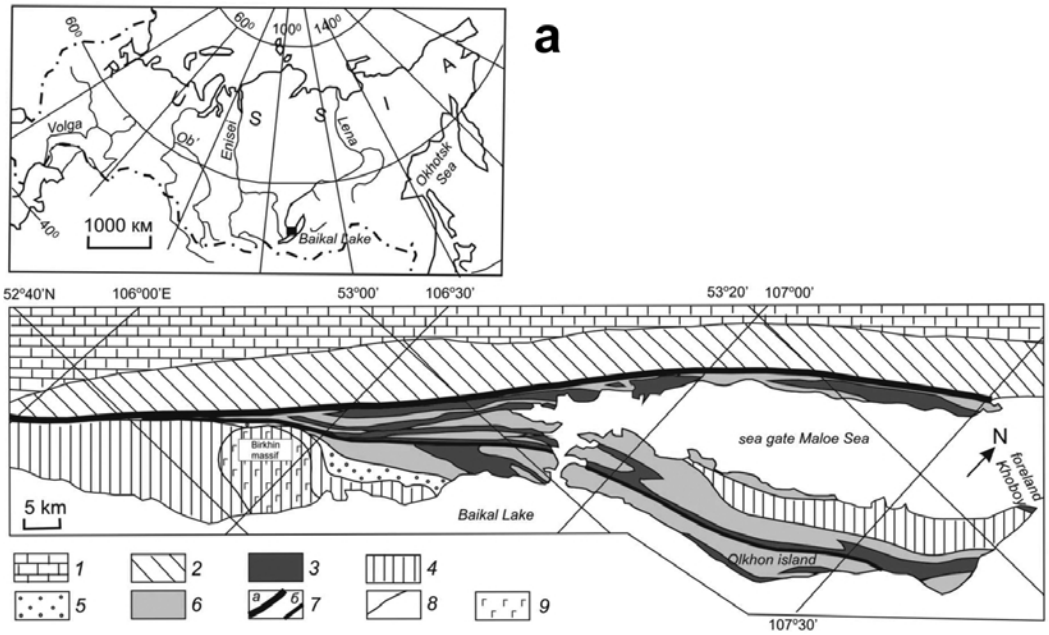
a
60°
100°
140°
Volga
Ob'
Enisei
Lena
Okhotsk Sea
40°
1000 км
Baikal Lake
52°40'N
106°00'E
53°00'
106°30'
53°20'
107°00'
Birkhin massif
5 km
Baikal Lake
sea gate Maloe Sea
N
foreland Khoboy
Olkhon island
107°30'
1
2
3
4
5
6
7
8
9

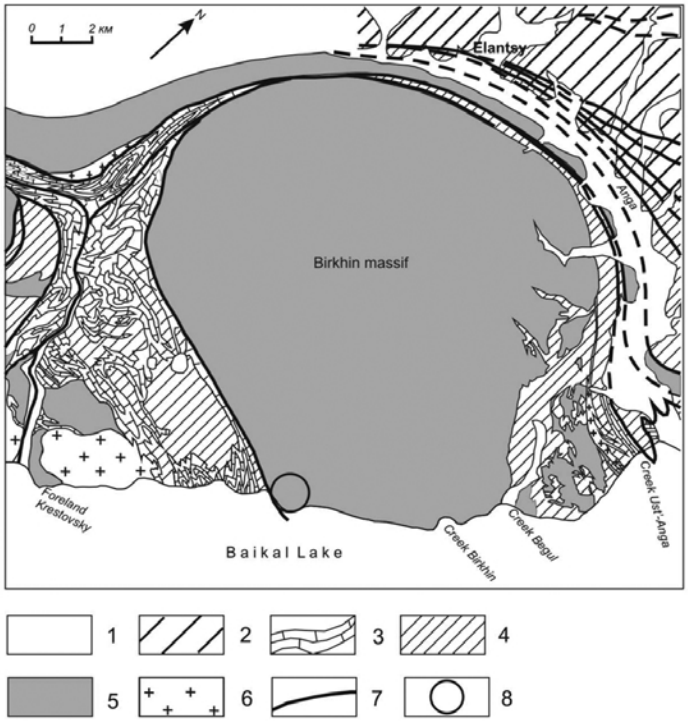
b
0 1 2 км
N
Élantsy
Birkhin massif
Angа
Foreland Krestovsky
Baikal Lake
Creek Birkhin
Creek Bagul
Creek Ust-Anga
1
2
3
4
5
6
7
8

recorded in backscatter geometry in the range 100–4000 cm^{-1} with a resolution of 2 cm^{-1}. Collection times of 20 s and an accumulation of five scans were used. The monochromator was calibrated using the Raman scattering line of a silicon plate (520.7 cm^{-1}).

Single crystal X-ray studies were carried out on several grains of Birkhin galuskinite using a Bruker APEX II SMART diffractometer (Mo-$K\alpha$ radiation, λ = 0.71073 Å). Details of the best crystal are summarized in Table 1. Diffraction data were collected with ω scans at different φ settings (φ-ω scan) (Bruker, 1999). Data were processed using the *SAINT* suite of software (Bruker, 1999). An empirical absorption correction using *SADABS* software (Sheldrick, 1996) was applied. The structure was solved by direct methods with subsequent analyses of difference-Fourier maps. The galuskinite structure was refined using the program *SHELX97* (Sheldrick, 2008) to R_1 = 3.1%. The 'best crystal' selected for structure solution and refinement consisted of more than one individual, intergrown in a more or less random fashion with admixed phases. Thus, the diffraction pattern of the major fragment had to be manually separated from the admixtures. The refinement [240 variable parameters, including anisotropic atom displacement parameters, 3287 $F_o > 4\sigma$ (F_o)] was carried out with neutral atom scattering factors. Due to scarcity of pure galuskinite the X-ray powder pattern was not measured but calculated from crystal structure data using the program *LAZY PULVERIX* (Yvon *et al*., 1977).

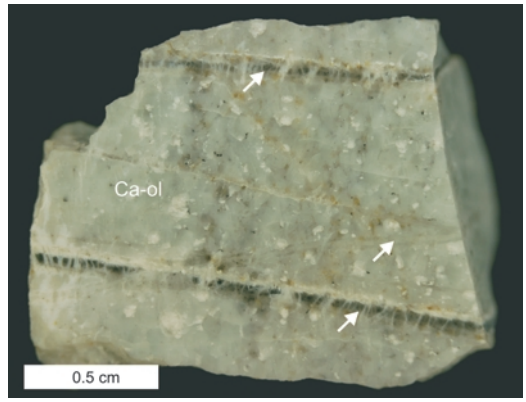

FIG. 2. Calcio-olivine (Ca-ol) skarn with veins containing galuskinite (arrowed).

Results

Macroscopic and microscopic mineral properties are summarized in Table 2. The small size and heterogeneity of galuskinite grains, which are found along fractures replaced by calcium hydrosilicates, meant that sample selection for straightforward determination of H_2O and CO_2 was not possible. However, Raman spectroscopy confirmed the presence of CO_3^{2-} in galuskinite (Fig. 4) and CO_3^{2-} was determined by single-crystal X-ray diffraction. There are no bands characteristic of OH in the Raman spectrum of galuskinite.

The electron microprobe analyses indicated only traces of Ti, K, Al, Mg, and Mn, which were not

FIG. 1 (*facing page*). Maps of the Olkhon collision zone. (*a*) Tectonic map of the Olkhon collision system (after Fedorovsky *et al*., 2010). The legend is as follows: (1,2) Siberian continental plate; (1) weakly deformed Riphean-Palaeozoic sedimentary cover, (2) Palaeoproterozoic metamorphic and granitic basement; (3–6) Early Palaeozoic collisional system, Olkhon composite terrane (stack of shear slabs composed of metamorphic and magmatic rocks of different age), (3) slabs formed by various metamorphic rocks including tholeitic basalts (500 Ma), (4) compositionally diverse metamorphic rocks with subalkaline basalts (500 Ma), (5) leptinite-amphibolite Orso complex, (6) slabs formed by granitic gneisses and migmatites (460–470 Ma) with signatures of Archaean-Palaeoproterozoic protolith; (7a) collision suture (margin of the Siberian craton and Olkhon terrane, blastomylonites composed of rocks of the craton and Olkhon terrane, among blastomylonites also erratic blocks of Palaeozoic granulites), (7b) main shear zone; (8) sutures of blastomylonites between shear zones; (9) Birkhin massif. (*b*) Geological map of the Birkhin massif (after Fedorovsky, 2004). The legend is as follows: (1) modern alluvium; (2) metamorphic rocks of the Olkhon complex; (3,4) metamorphic rocks of the Angin complex (including the Orso complex), (3) marble, (4) other metamorphic rock (meta-effusive rock of intermediate and mafic composition, metabreccia, quartzite, highly aluminous rocks, garnet-biotite gneiss, marble melange); (5) gabbro, monzogabbro, diorite and their metamorphosed analogues; (6) granite; (7) syn-metamorphic blastomylonite shear zones and thrust faults; (8) area of work.

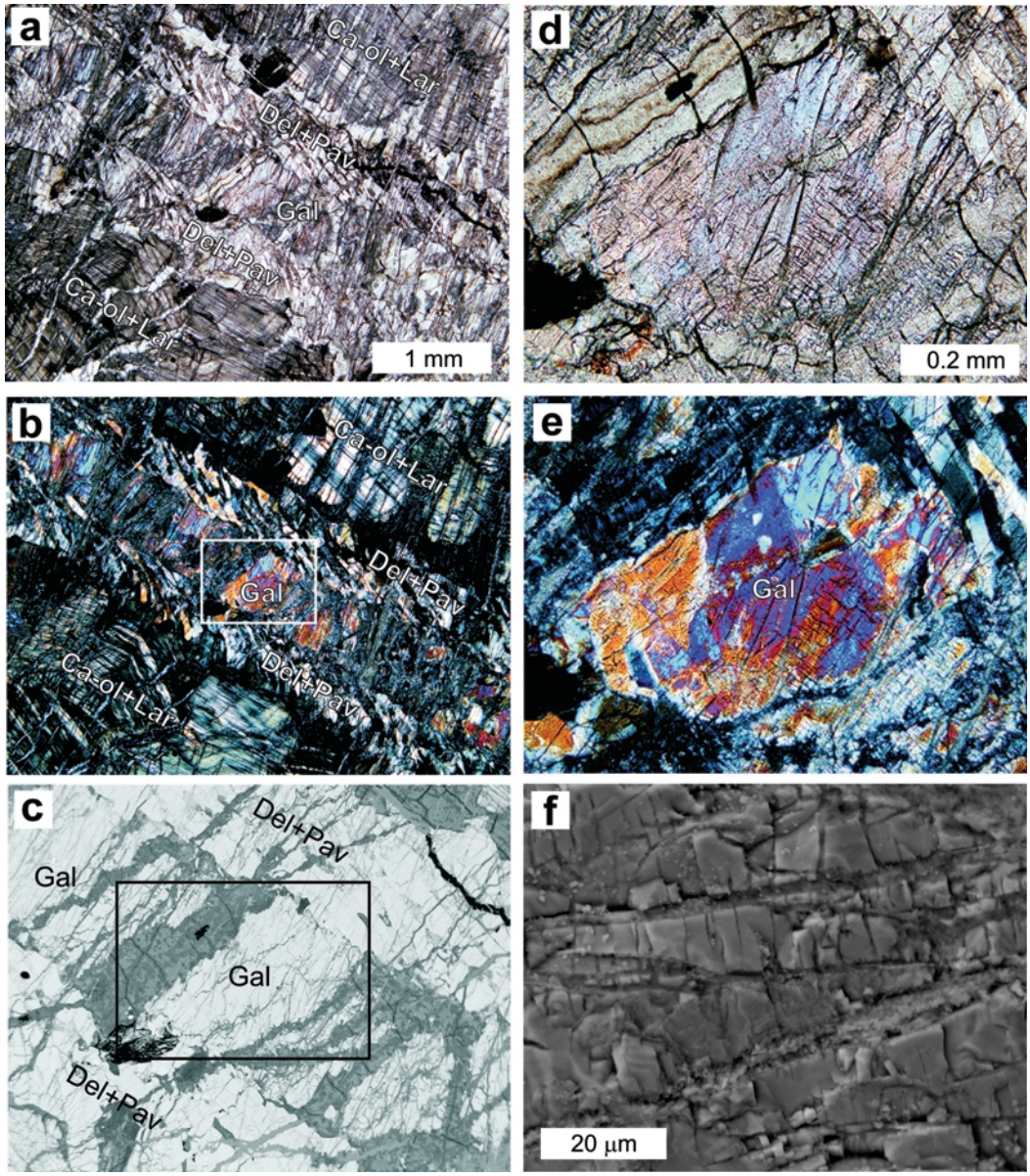

FIG. 3. Galuskinite (Gal) fills the central part of veins in calcio-olivine (Ca-ol). Borders of the veins are represented by aggregates of dellaite (Del) and pavlovskyite (Pav): (*a*–*c*) overviews; (*d*,*e*) magnified portions of the central part shown in (*b*) and (*c*); (*f*) the parting character of galuskinite; (*a*,*d*) are in plane polarized light; (*b*,*e*) are with crossed polarizers; (*c*,*f*) are back scattered electron images.

quantified; both B and F were below detection limits. Analytical data are given in Table 3. The empirical formula (based on 15 O atoms) is $(Ca_{6.936}Na_{0.086})_{\Sigma 7.022}(Si_{2.983}P_{0.018}S_{0.004})_{\Sigma 3.005}O_{12}(CO_3)$. The simplified formula is $Ca_7(SiO_4)_3(CO_3)$, which corresponds to: CaO, 63.63 wt.%; SiO_2, 29.22 wt.% and CO_2, 7.14 wt.%.

The results of the crystal structure refinement including atomic coordinates and isotropic equivalents (U_{eq}) of anisotropic atom displacement

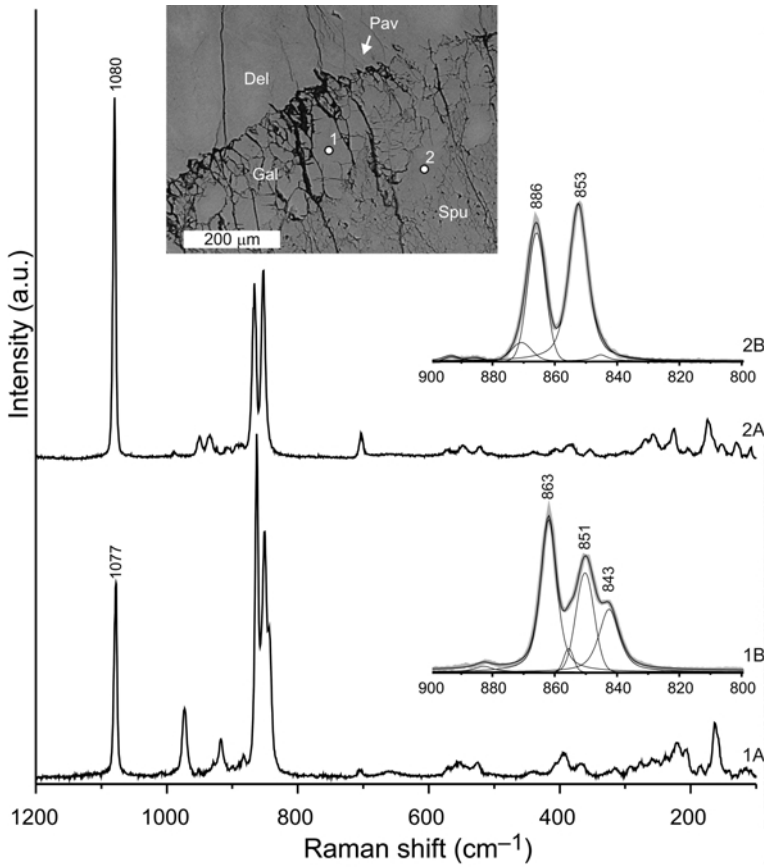

FIG. 4. The Raman spectrum of galuskinite (1A and 1B) in comparison with the corresponding spectrum for spurrite (2A and 2B). The points where the Raman measurements were made are shown on inset photo which shows replacement of dellaite by galuskinite and galuskinite by spurrite.

parameters are listed in Table 4, anisotropic displacement parameters in Table 5 and selected interatomic distances in Table 6. Final difference-Fourier maps showed a peak of 1.5 e/Å^3, which was refined as a partly occupied H_2O site (OW). However, there are no bands which are characteristic of either OH or H_2O in the Raman spectrum of galuskinite, so it seems more probable that this peak is an artefact produced by intensity contributions from non-corrected admixtures. The close proximity of this 'ghost peak' to the C-site at 2.56 Å makes its relevance to the structure of galuskinite rather unlikely. The refinement quality of other galuskinite crystals studied was considerably poorer and the weak 'ghost peak' was not detected. Calculated X-ray powder data for Debye-Scherrer geometry and Cu-$K\alpha$ radiation are presented in Table 7 and Fig. 5.

Discussion

Formation conditions

The original skarn assemblage of larnite, (calcio-olivine) and bredigite combined with the enclosed minerals, indicates sanidinite facies conditions (low pressure and temperature above 800ºC). The presence of pavlovskyite and dellaite, which form the margin between the high-temperature skarn and galuskinite, may indicate secondary hydration reactions at temperatures in the range of 350–600ºC (Agrell, 1965; Bennett *et al*. 1966; Speakman *et al*., 1967; Garbev *et al*., 2008; Shimazaki *et al*., 2008). Galuskinite replaces dellaite and is subsequently replaced by spurrite (Fig. 4, inset). It may be speculated that galuskinite formed in a similar temperature range when reactive CO_2 entered the vein

TABLE 1. Parameters for X-ray data collection and crystal-structure refinement for galuskinite.

Crystal data	
Unit cell dimensions (Å)	a = 18.7872(5) b = 6.7244(2) c = 10.4673(2) β = 90.7880(10)º
Volume (Å^3)	1322.24(6)
Space group	$P2_1/c$ No. 14
Z	4
μ (mm^{-1})	3.2
Intensity measurement	
Crystal shape	Prismatic
Crystal size (mm)	0.12 × 0.12 × 0.16
Diffractometer	APEX II SMART
X-ray radiation	Mo-$K\alpha$ λ = 0.71073 Å
X-ray power	50 kV, 30 mA
Monochromator	Graphite
Temperature	293 K
Detector to sample distance	5.95 cm
Measurement method	Psi-omega scans
Rotation width	0.5º
Frame size	512 × 512 pixels
Time per frame	120 sec
θ-range for data collection	2.2 to 30.5º
Index ranges	$-26 \leqslant h \leqslant 26$ $-8 \leqslant k \leqslant 9$ $-14 \leqslant l \leqslant 14$
No. of measured reflections	20642
No. of unique reflections	4039
No. of observed reflections ($I > 2\sigma(I)$)	3287
Refinement of the structure	
No. of parameters refined	240
R_{int}	0.0592
R_σ	0.0388
$R1$, $I > 2\sigma(I)$	0.0310
$R1$, all data	0.0433
w$R2$ (on F^2)	0.0737
GooF	1.055
$\Delta\rho_{min}$ (−e. Å^{-3})	−0.65 close to Si1
$\Delta\rho_{max}$ (e. Å^{-3})	0.70 close to Ca2

system. Most surprisingly, the synthetic analogue of galuskinite is not known.

Modular structure of galuskinite

Galuskinite is an orthosilicate with additional CO_3 groups. There are seven symmetry-independent Ca sites with O coordination of between seven and eight. The arrangement of the coordination polyhedra indicates a modular character with strong structural similarities to spurrite and larnite. The layer concept of calcium silicate carbonate introduced by Grice (2005) is the basis for the modular interpretation and has here been extended to larnite. To better understand the galuskinite structure the modular components are discussed first.

The larnite structure, β-Ca_2SiO_4, space group $P2_1/n$ [a = 5.502, b = 6.745, c = 9.297 Å, β = 94.59º, V = 344 Å^3; Jost *et al*., 1977] is composed of tightly interwoven layers (Fig. 6). The layers extend parallel to (10$\bar{1}$) and are formed by sevenfold coordinated Ca1 (distorted pentagonal dipyramids) and eight-fold coordinated Ca2

TABLE 2. Properties of galuskinite.

Property	
Habit	Aggregates of highly fractured grains
Forms	Not determined
Twinning	Simple and polysynthetic twins on (001)
Colour	Colourless, white, pale grey
Streak	White
Lustre	Vitreous, transparent
Fluorescence	Not observed
Hardness	H (Mohs): ~5; VHN load 20 g, mean (3) = 440 kg mm^{-2}
Tenacity	Brittle
Cleavage	Imperfect on (001), (100), and (010)
Parting	Perfect on (001)
Fracture	Uneven
Density (calc.)	3.096 g cm^{-3}
Optical properties	Not pleochroic
α (589 nm)	1.660(3)
β (589 nm)	1.669(3)
γ (589 nm)	1.676(3)
$2V_x$ obs/calc	60(5)º / 82.4
Optical orientation (difficult to determine: undulatory extinction)	$\alpha \parallel b$, $\gamma \wedge a \approx 25º$, $\beta \wedge c \approx 25º$ or $\alpha \parallel b$, $\gamma \wedge c \approx 25º$, $\beta \wedge a \approx 25º$
Compatibility $1 - (K_p/K_c)$:	−0.031 (excellent).

(dodecahedra = 'anticubes'). Interspersed amongst the Ca polyhedra are SiO_4 tetrahedra, which are linked on their triangular face to the layer of Ca polyhedra. All three edges of this triangle are edge-connected with Ca polyhedra. The back and front sides of the layer are related by a 2_1 axis parallel to *b*. The layers have $2 \times Ca_2SiO_4$ composition.

TABLE 3. Analytical data for galuskinite (mean of 60 results).

Oxides	Wt.%	SD	Range
SiO_2	28.85	0.29	28.40−29.94
CaO	62.61	0.43	61.73−63.62
Na_2O	0.43	0.05	0.33−0.54
SO_3	0.05	0.03	0−0.14
P_2O_5	0.20	0.09	0.04−0.43
CO_2*	7.08		
Total	99.22		

* Calculated by stoichiometry from the results of the crystal structure analysis.

Spurrite, $Ca_5(SiO_4)_2CO_3$, space group $P2_1/a$ (a = 10.48, b = 6.71, c = 14.16 Å, β = 101.27º, V = 977 $Å^3$; e.g. Grice (2005)) can be considered to consist of tightly interwoven layers parallel to (001) (Fig. 7). Two different types of layers can be distinguished. The central layer, with a Ca_2SiO_4 composition, contains eight-coordinate polyhedra around Ca2 and Ca3, which are linked by their edges with SiO_4 (Si2) tetrahedra. Thus each tetrahedron has two connected edges. The second type of layer looks like a larnite module on the front side but on the reverse side it is different. The layer-forming Ca coordination polyhedra are 7- and 8-fold coordinated but topologically opposite to the larnite module. This reversal of coordination is not apparent on the larnite-like side but it is responsible for the altered topology of the back side of the module, which has CO_3 linked with one edge to eight-coordinate Ca1. The bonding of CO_3 with a low Lewis-base strength to eight-coordinate Ca (low Lewis-acid strength) is in accordance with the valence matching principle (Brown, 2002). The free CO_3 apex joins this module to the central layer. The mixed anion layer (Ca1, Ca4, Ca5, Si1, C1) has the composition Ca_2SiO_4+$CaCO_3$.

TABLE 4. Atomic coordinates and isotropic equivalents (U_{eq}) of anisotropic atom displacement parameters of galuskinite.

Site	Atom	*x*	*y*	*z*	U_{eq}	Occupancy
Ca1	Ca	0.25320(3)	0.99544(8)	0.03445(5)	0.01055(10)	1
Ca2	Ca	0.00225(3)	0.49318(8)	−0.29336(5)	0.01029(10)	1
Ca3	Ca	0.46782(3)	0.94041(8)	0.25248(5)	0.01130(11)	1
Ca4	Ca	0.18601(3)	0.34203(8)	0.24622(6)	0.01206(11)	1
Ca5	Ca	−0.08011(3)	0.34023(8)	−0.00397(6)	0.01214(11)	1
Ca6	Ca	0.41771(3)	0.23372(8)	−0.00793(6)	0.01298(11)	1
Ca7	Ca	0.26033(3)	0.51157(8)	−0.05254(5)	0.01028(10)	1
Si1	Si	0.42237(3)	0.74899(10)	−0.00051(7)	0.00795(13)	1
Si2	Si	0.17238(4)	0.71963(10)	−0.25559(7)	0.00809(13)	1
Si3	Si	0.09001(4)	0.22209(10)	0.00646(7)	0.00823(13)	1
O1	O	0.37171(10)	0.9182(3)	0.0636(2)	0.0138(4)	1
O2	O	0.37975(10)	0.5666(3)	−0.06914(19)	0.0122(4)	1
O3	O	0.52592(10)	0.1483(3)	0.10652(19)	0.0128(4)	1
O4	O	0.47714(10)	0.6661(3)	0.10925(19)	0.0117(4)	1
O5	O	0.20363(10)	0.0054(3)	0.23703(19)	0.0113(3)	1
O6	O	0.21195(11)	0.8270(3)	−0.1359(2)	0.0142(4)	1
O7	O	−0.08658(10)	0.2693(3)	0.2339(2)	0.0133(4)	1
O8	O	−0.19184(10)	0.3392(3)	−0.11325(19)	0.0128(4)	1
O9	O	0.07252(10)	0.9886(3)	0.0047(2)	0.0141(4)	1
O10	O	0.17363(10)	0.2609(3)	−0.0245(2)	0.0127(4)	1
O11	O	0.03815(10)	0.3388(3)	−0.09493(19)	0.0127(4)	1
O12	O	0.07182(10)	0.3198(3)	0.14611(19)	0.0129(4)	1
O13	O	0.30111(10)	0.3108(3)	0.13532(19)	0.0131(4)	1
O14	O	0.30607(10)	0.3051(3)	0.3491(2)	0.0133(4)	1
O15	O	0.40565(10)	0.2799(3)	0.2365(2)	0.0159(4)	1
C1	C	0.33806(13)	0.3005(4)	0.2405(3)	0.0113(5)	1
OW	O	0.3372(12)	0.681(4)	0.253(2)	0.028(7)	0.109(9)

The galuskinite structure, $Ca_7(SiO_4)_3CO_3$, space group $P2_1/c$ (a = 18.79, b = 6.72, c = 10.47 Å, β = 90.79°, V = 1322 Å^3; this paper) may also be interpreted as being built from intimately connected layers parallel to (100) (Fig. 8). Three different types of layers can be distinguished. The central layer of Ca_2SiO_4 composition is assembled from eight-coordinate polyhedra around Ca3 and Ca6, which are linked by their edges with SiO_4 (Si1) tetrahedra. Thus each tetrahedron has two connected edges. This module is identical to the central module in spurrite. The Ca6 site may be interpreted as nine-coordinate (Table 6), however, the ninth oxygen ligand, which is 2.969 Å away, is a similar distance to Ca6−C. For this reason and because of structural similarities to spurrite, an eight-fold coordination of the Ca6 position is used in this comparative discussion. The second type of layers looks like the larnite module on the front side but on the reverse side CO_3 triangles are present. Thus the CO_3-bearing module corresponds to the one in spurrite. This mixed anion layer (Ca1, Ca4, Ca7, Si2, C1) has the composition Ca_2SiO_4 + $CaCO_3$. An additional larnite module (Ca2, Ca5, Si3) completes the stacking sequence along *a*. If the unit-cell volumes of larnite (Jost *et al*., 1977) and spurrite (Grice, 2005) are added (1321 Å^3) the unit-cell volume of galuskinite is obtained. This close resemblance indicates that the modular daughter structure (galuskinite) is very similar to the parent structures of larnite and spurrite with regard to space filling and polyhedral distortions.

One may also define a polysomatic series with spurrite and larnite as the endmembers, and with galuskinite as a 1:1 polysome built by regularly alternating spurrite and larnite modules. The structures of spurrite (Grice, 2005) and larnite (Jost *et al*., 1977) may be easily re-oriented so that there are common values for the *b* and *c* parameters and the same space group setting $P2_1/c$: galuskinite: a = 18.79, b = 6.72,

TABLE 5. Anisotropic displacement parameters for galuskinite.

Site	U_{11}	U_{22}	U_{33}	U_{23}	U_{13}	U_{12}
Ca1	0.0119(2)	0.0096(2)	0.0101(2)	−0.00121(18)	0.00086(17)	0.00018(17)
Ca2	0.0112(2)	0.0092(2)	0.0105(2)	−0.00053(19)	0.00147(17)	−0.00087(16)
Ca3	0.0150(2)	0.0093(2)	0.0096(3)	−0.00016(18)	0.00180(18)	0.00025(17)
Ca4	0.0124(2)	0.0097(2)	0.0141(3)	−0.00007(19)	−0.00002(19)	0.00056(17)
Ca5	0.0130(2)	0.0086(2)	0.0148(3)	−0.00061(19)	0.00017(19)	0.00061(17)
Ca6	0.0099(2)	0.0152(2)	0.0139(3)	0.0051(2)	0.00050(18)	−0.00049(18)
Ca7	0.0097(2)	0.0095(2)	0.0117(3)	−0.00014(19)	0.00092(17)	0.00051(16)
Si1	0.0080(3)	0.0075(3)	0.0083(3)	0.0000(2)	0.0009(2)	0.0004(2)
Si2	0.0092(3)	0.0068(3)	0.0083(3)	0.0001(2)	0.0014(2)	−0.0003(2)
Si3	0.0082(3)	0.0071(3)	0.0093(3)	−0.0002(2)	0.0011(2)	−0.0002(2)
O1	0.0127(8)	0.0130(9)	0.0158(10)	−0.0016(8)	0.0015(7)	0.0041(7)
O2	0.0106(8)	0.0117(8)	0.0143(10)	−0.0016(7)	0.0012(7)	−0.0020(6)
O3	0.0141(8)	0.0144(9)	0.0099(10)	0.0016(7)	0.0024(7)	−0.0036(7)
O4	0.0117(8)	0.0113(8)	0.0120(10)	0.0017(7)	0.0007(7)	0.0020(6)
O5	0.0145(8)	0.0082(8)	0.0113(9)	0.0001(7)	0.0014(7)	−0.0019(6)
O6	0.0174(9)	0.0125(9)	0.0127(10)	−0.0032(7)	−0.0031(7)	0.0010(7)
O7	0.0102(8)	0.0114(9)	0.0184(11)	0.0001(8)	0.0015(7)	0.0000(6)
O8	0.0159(9)	0.0107(9)	0.0118(10)	−0.0016(7)	0.0011(7)	0.0021(7)
O9	0.0148(9)	0.0097(8)	0.0180(10)	−0.0003(8)	0.0016(7)	−0.0013(7)
O10	0.0097(8)	0.0119(8)	0.0166(10)	0.0012(7)	0.0017(7)	−0.0016(6)
O11	0.0131(8)	0.0132(9)	0.0119(10)	0.0025(7)	−0.0003(7)	0.0012(6)
O12	0.0139(8)	0.0129(9)	0.0119(10)	−0.0022(7)	0.0021(7)	0.0010(7)
O13	0.0147(8)	0.0130(9)	0.0116(10)	0.0013(7)	−0.0008(7)	0.0001(7)
O14	0.0125(8)	0.0137(9)	0.0137(10)	−0.0012(7)	0.0015(7)	0.0000(7)
O15	0.0111(8)	0.0174(10)	0.0191(11)	−0.0004(8)	0.0015(7)	0.0008(7)
C1	0.0098(10)	0.0120(11)	0.0122(13)	0.0001(9)	0.0007(9)	0.0007(8)

c = 10.47 Å, β = 90.79°; spurrite: a = 14.156, b = 6.71, c = 10.484 Å, β = 101.27°, is transformed by [001/010/100]; larnite: a = 5.502, b = 6.745, c = 10.417 Å, β = 117.18°, is transformed by [$\bar{1}$00/010/101]. Using these values, the a periodicity of galuskinite is obtained easily from those of spurrite and larnite: 18.79 Å × sin 90.79° = 14.156 Å × sin 101.25° + 5.502 Å × sin 117.18°.

For a 1:1 polysome like galuskinite, the physical properties may be predicted from the properties of the endmembers. Synthetic spurrite has refractive indices α = 1.638(2), β = 1.670(2), γ = 1.676(2) (Tuttle and Harker, 1957) and larnite has α = 1.707, β = 1.715, γ = 1.730 (Tilley, 1929); the optical properties of galuskinite are summarized in Table 2. As the unit-cell volumes of spurrite and larnite have a 2.8:1 ratio, the calculated refractive indices have to be weighted by this ratio. In spurrite and galuskinite α is parallel to b, whereas in larnite γ is parallel to b. Structures with CO_3 aligned in parallel fashion usually have their lowest refractive indices perpendicular to the planar CO_3 group (b in galuskinite and spurrite). The weighted refractive index parallel to b (α) in galuskinite is thus predicted to be 1.662, which is in good agreement with the measured value of 1.660(3) (Table 2). Due to uncertainty in the exact optical orientation for galuskinite (Table 2) only average values will be considered for the remaining refractive indices within the plane of the CO_3 group. The value of galuskinite for (β + γ)/2 is predicted to be 1.684, which is slightly higher than the measured value of 1.673. Spurrite has a SiO_4:CO_3 ratio of 2:1 whereas galuskinite has 3:1. Thus the anisotropic CO_3 coordination must have a stronger influence on the optical properties of spurrite resulting in a higher optical birefringence (δ = 0.038) than determined for galuskinite (δ = 0.016).

Relation to other skarn minerals

Due to the close structural similarities between galuskinite and spurrite, the X-ray powder patterns of the two minerals are strikingly similar in the high-2θ region. However, in the

TABLE 6. Selected interatomic distances (Å) in galuskinite.

$^{[VII]}$Ca1	$^{[IX]}$Ca6
−O6 2.242(2)	−O4 2.3533(19)
−O1 2.3024(19)	−O1 2.414(2)
−O5 2.329(2)	−O3 2.415(2)
−O10 2.404(2)	−O2 2.433(2)
−O13 2.529(2)	−O14 2.573(2)
−O14 2.570(2)	−O15 2.590(2)
−O8 2.664(2)	−O15 2.684(2)
Mean Ca1−O: 2.434	−O13 2.721(2)
	−O3 2.969(2)
$^{[VIII]}$Ca2	Mean Ca6−O: 2.572
−O7 2.328(2)	
−O11 2.410(2)	$^{[VII]}$Ca7
−O12 2.440(2)	−O2 2.2830(19)
−O7 2.4484(19)	−O10 2.3650(19)
−O9 2.510(2)	−O8 2.395(2)
−O12 2.562(2)	−O5 2.436(2)
−O9 2.605(2)	−O6 2.463(2)
−O11 2.705(2)	−O13 2.497(2)
Mean Ca2−O: 2.501	−O14 2.521(2)
	Mean Ca7−O: 2.422
$^{[VIII]}$Ca3	
−O4 2.330(2)	Si1
−O3 2.351(2)	−O2 1.626(2)
−O4 2.385(2)	−O4 1.630(2)
−O3 2.459(2)	−O1 1.633(2)
−O2 2.512(2)	−O3 1.638(2)
−O15 2.569(2)	Mean Si1−O: 1.632
−O15 2.612(2)	
−O1 2.664(2)	Si2
Mean Ca3−O: 2.485	−O6 1.618(2)
	−O5 1.625(2)
$^{[VII]}$Ca4	−O7 1.6327(19)
−O5 2.2900(19)	−O8 1.637(2)
−O12 2.379(2)	Mean Si2−O: 1.627
−O13 2.477(2)	
−O14 2.498(2)	Si3
−O10 2.512(2)	−O9 1.604(2)
−O8 2.559(2)	−O10 1.6294(19)
−O6 2.588(2)	−O11 1.632(2)
Mean Ca4−O: 2.473	−O12 1.643(2)
	Mean Si3−O: 1.627
$^{[VII]}$Ca5	
−O9 2.216(2)	C
−O8 2.377(2)	−O15 1.279(3)
−O11 2.429(2)	−O14 1.293(3)
−O11 2.516(2)	−O13 1.295(3)
−O7 2.539(2)	Mean C−O: 1.289
−O12 2.733(2)	
−O7 2.842(2)	
Mean Ca5−O: 2.522	

TABLE 7. Calculated X-ray powder pattern for galuskinite. Only intensities >5 are listed. The ten strongest lines are in bold.

h	*k*	*l*	*d*	I_{rel}	*h*	*k*	*l*	*d*	I_{rel}
1	**0**	**0**	**18.7854**	**56**	4	1	$\bar{4}$	2.1756	21
2	0	0	9.3927	15	4	1	4	2.1529	16
1	1	0	6.3310	17	4	2	3	2.1435	9
3	0	0	6.2618	34	3	3	0	2.1103	6
2	1	0	5.4676	13	1	3	2	2.0469	7
0	0	2	5.2332	26	7	1	$\bar{3}$	2.0404	22
2	1	1	4.8304	7	6	0	$\bar{4}$	2.0215	9
4	0	0	4.6964	19	7	1	3	2.0159	7
3	0	$\bar{2}$	4.0429	21	2	3	$\bar{2}$	2.0149	6
3	0	2	3.9886	9	2	3	2	2.0103	6
4	1	0	3.8503	16	0	1	5	1.9987	6
2	1	$\bar{2}$	3.7958	15	6	0	4	1.9943	5
2	1	2	3.7656	10	9	1	0	1.9934	7
5	0	0	3.7571	12	1	1	$\bar{5}$	1.9902	24
4	0	$\bar{2}$	3.5194	6	9	1	$\bar{1}$	1.9630	14
4	0	2	3.4716	8	**8**	**2**	**0**	**1.9251**	**53**
0	2	0	3.3622	15	6	2	3	1.9064	5
5	1	0	3.2799	5	4	2	$\bar{4}$	1.8979	20
0	2	1	3.2011	26	8	2	$\bar{1}$	1.8972	5
2	2	0	3.1655	6	3	1	5	1.8968	6
1	2	1	3.1534	5	4	2	4	1.8828	24
5	1	$\bar{1}$	3.1406	21	0	2	5	1.7770	6
6	0	0	3.1309	16	5	1	$\bar{5}$	1.7742	16
5	0	$\bar{2}$	3.0721	16	8	0	$\bar{4}$	1.7597	6
1	1	3	3.0496	26	11	0	0	1.7078	9
5	**0**	**2**	**3.0323**	**59**	3	2	5	1.7043	11
2	2	1	3.0261	9	7	3	1	1.6952	6
3	2	0	2.9622	20	9	2	$\bar{2}$	1.6855	7
2	1	$\bar{3}$	2.9518	6	0	4	0	1.6811	9
3	2	1	2.8454	8	5	3	3	1.6804	6
4	**2**	**0**	**2.7338**	**98**	8	2	3	1.6776	6
2	**2**	$\bar{\mathbf{2}}$	**2.7141**	**78**	9	2	2	1.6736	8
6	**0**	$\bar{\mathbf{2}}$	**2.7032**	**100**	0	2	0	1.6399	7
2	**2**	**2**	**2.7030**	**85**	6	3	$\bar{3}$	1.6207	6
6	**0**	**2**	**2.6706**	**100**	5	2	$\bar{5}$	1.6137	7
0	**0**	**4**	**2.6166**	**82**	12	0	0	1.5655	8
4	1	3	2.5709	12	10	2	2	1.5596	9
6	1	2	2.4820	11	8	2	$\bar{4}$	1.5591	5
3	0	$\bar{4}$	2.4262	7	7	3	$\bar{3}$	1.5484	9
0	2	3	2.4209	19	1	3	$\bar{5}$	1.5261	7
8	0	0	2.3482	7	6	0	6	1.5150	10
2	2	3	2.3389	7	6	4	$\bar{2}$	1.4276	5
3	2	$\bar{3}$	2.2653	43	7	4	0	1.4247	5
1	3	0	2.2257	6	6	4	2	1.4227	7
8	1	0	2.2169	13	0	4	4	1.4143	10
0	3	1	2.1918	6	12	0	$\bar{4}$	1.3516	5
6	1	3	2.1884	13	12	0	4	1.3353	8
2	3	0	2.1802	7	0	0	8	1.3083	6
1	**3**	$\bar{\mathbf{1}}$	**2.1777**	**52**					

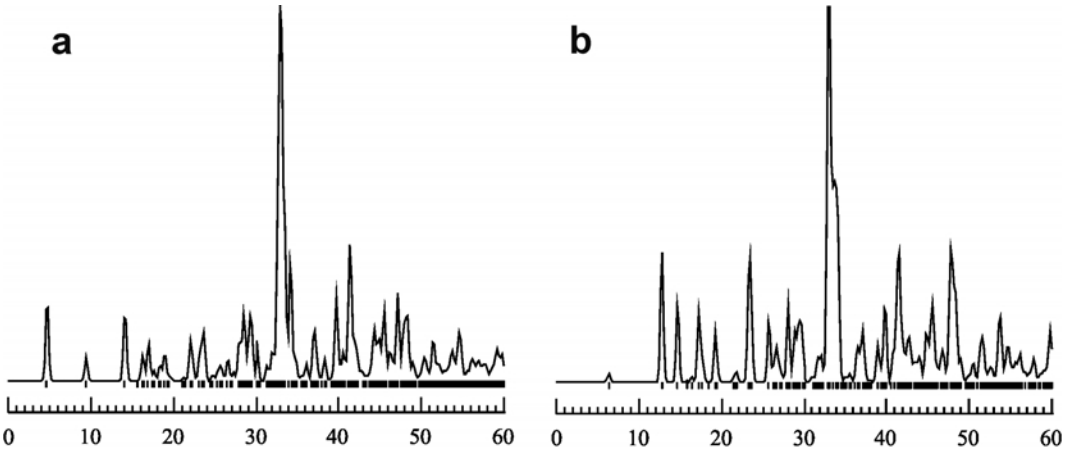

FIG. 5. Calculated X-ray powder patterns (Cu-$K\alpha$ 2θ) from *Atoms 5.1* by Shape Software: (*a*) galuskinite; (*b*) spurrite (Grice, 2005). Differences are most obvious in the low 2θ region.

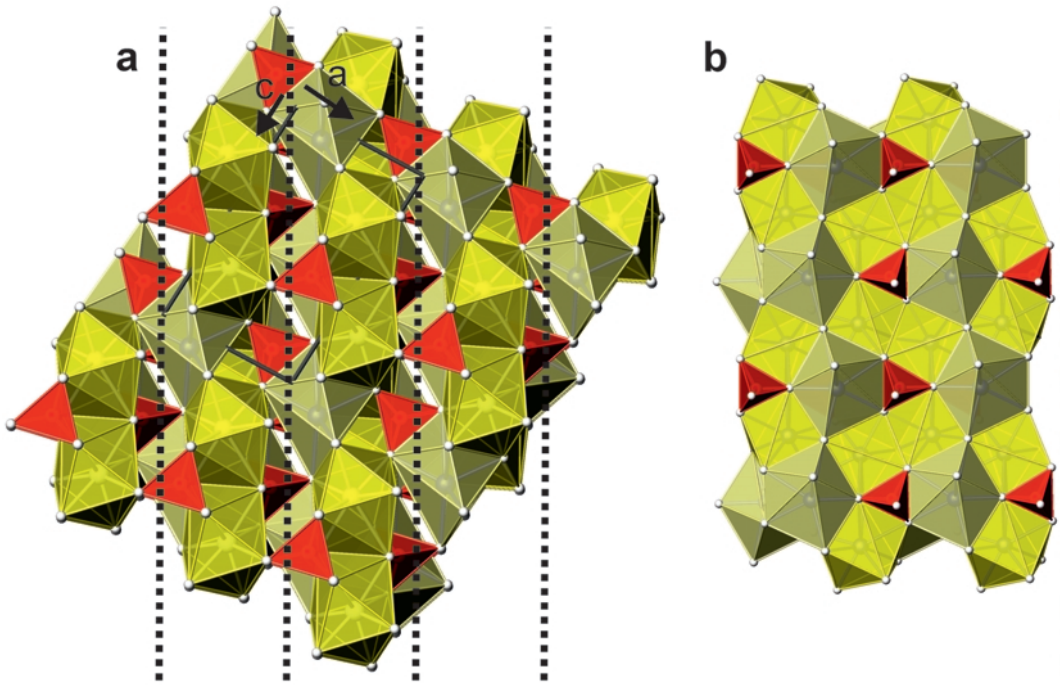

FIG. 6. Polyhedral model of the crystal structure of larnite. (*a*) Projection of the structure along *b* with unit-cell outlines. Dashed contours intersect the structure in layered modules parallel to $(10\bar{1})$. (*b*) Isolated $(10\bar{1})$ larnite module (*b* horizontal). The layer module is composed of pale yellow Ca polyhedra with 7-fold coordination, intense yellow Ca dodecahedra (8-fold coordination) and red SiO_4 tetrahedra in a ratio of 1:1:1. Corresponding SiO_4 tetrahedra and 7-coordinate Ca occur on the front and reverse sides of the layer.

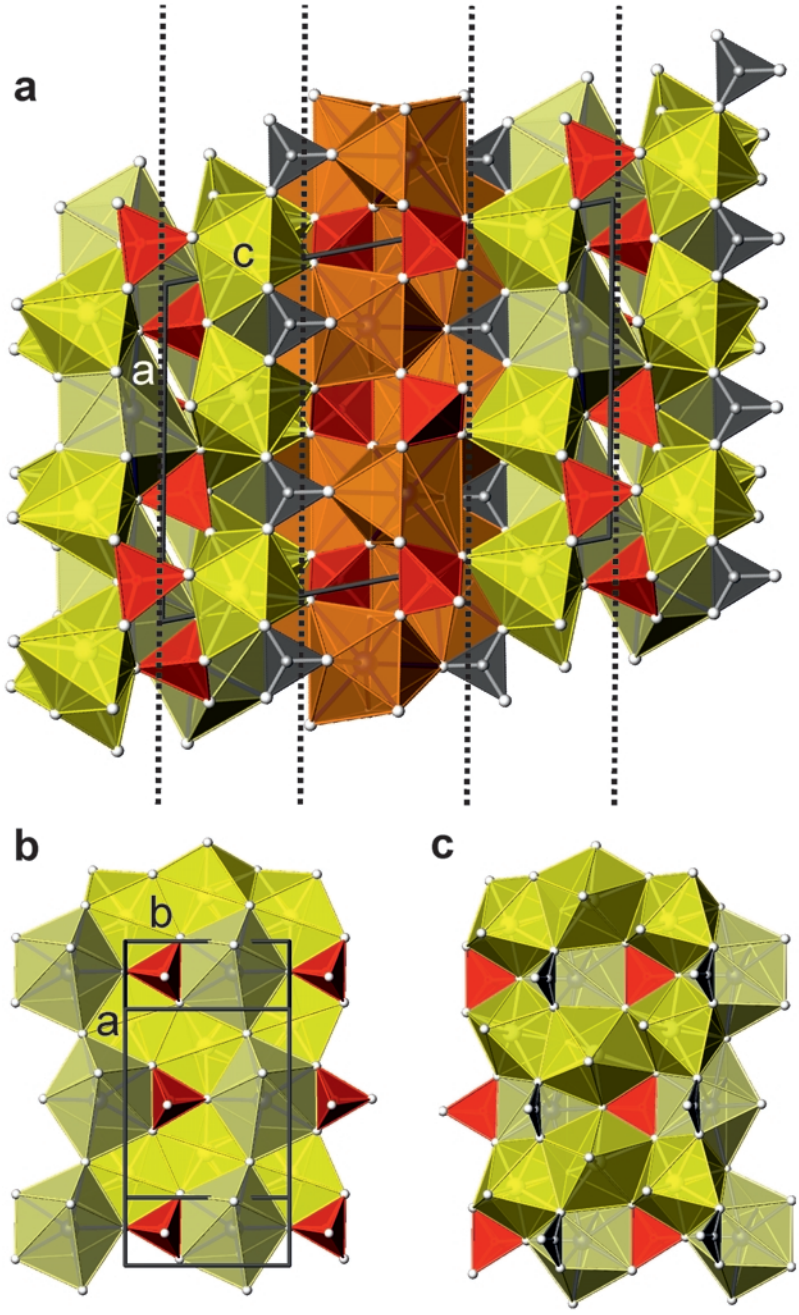

FIG. 7. Polyhedral model of the crystal structure of spurrite. (*a*) Projection of the structure along *b* with unit-cell outlines. Dashed contours intersect the structure in layered modules parallel to (001). (*b*) Isolated (001) front side of a module resembling the larnite module (*b* horizontal). The layer module is composed of pale yellow Ca polyhedra with 8-fold coordination, intense yellow Ca polyhedra (7-fold coordination) and red SiO_4 tetrahedra in a ratio of 1:1:1. (*c*) Reverse of the same module (slightly tilted for better visibility of triangular (dark grey) CO_3 units). This mixed anion layer has a Ca_2SiO_4+$CaCO_3$ composition.

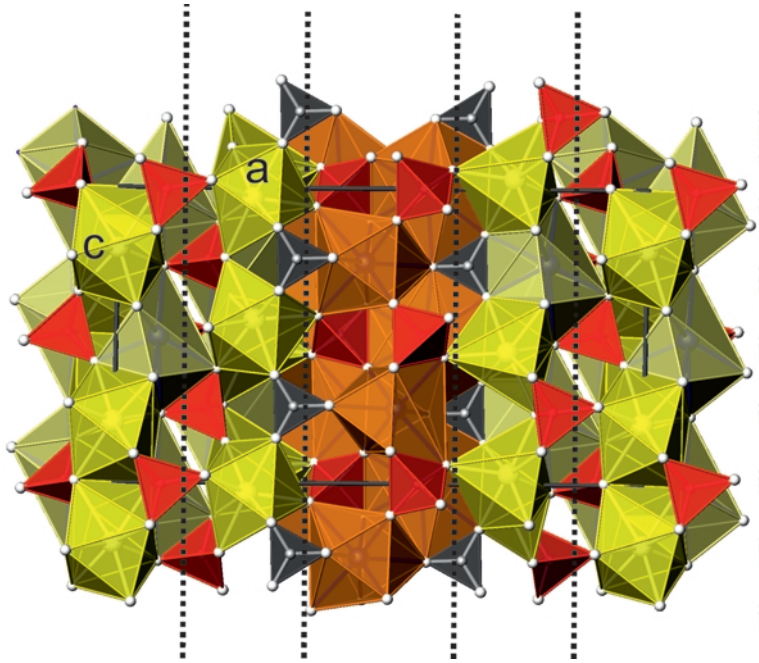

FIG. 8. Polyhedral model of the crystal structure of galuskinite with colours as in Figs 6 and 7. The projection of the structure is along *b* with unit cell outlines. Dashed lines intersect the structure in layered modules parallel to (100). The structure is composed of a central module (orange eight-coordinate Ca polyhedra with red SiO_4 tetrahedra, module composition Ca_2SiO_4) analogous to spurrite, followed by a layer with a topologically different front (Ca_2SiO_4) and reverse ($CaCO_3$) as found in spurrite. The sequence is completed by one perfect larnite layer of Ca_2SiO_4 composition. Adding up the modular units, the composition of galuskinite is $Ca_7(SiO_4)_3CO_3$.

low-2θ region there are significant differences. A diagnostic feature of galuskinite is the first diffraction peak at d = 18.78 Å (1 0 0; I = 56%); the first diffraction peak of spurrite is at d = 13.88 Å (0 0 1; I = 5%) and is considerably weaker (Fig. 5).

Galuskin *et al*. (2009) described another new skarn mineral with the same Ca:Si ratio of 7:3, which was named chegemite, $Ca_7(SiO_4)_3(OH)_2$. Chegemite is the calcium hydroxyl analogue of humite and is therefore structurally related to calcio-olivine, γ-Ca_2SiO_4. Thus, chegemite is an orthosilicate with Ca in octahedral coordination. Endmember chegemite has the composition 66.44 wt.% CaO, 30.51 wt.% SiO_2 and 3.05 wt.% H_2O whereas galuskinite is 63.63 wt.% CaO, 29.22 wt.% SiO_2 and 7.14 wt.% CO_2. If only the heavy elements are considered the two minerals are easily confused, however, the Raman spectrum (Fig. 4) and X-ray diffraction pattern enable unambiguous identification.

Acknowledgements

The authors thank Prof. Leonid Dubrovinsky, Bayerisches Geoinstitut, Universität Bayreuth, Germany, for Raman spectroscopic investigations. Evgeny Galuskin and Irina Galuskina are thanked for their help characterizing the new mineral. We would also like to thank the reviewers Stefano Merlino (Pisa) and Herta Effenberger (Vienna) as well as the editors for their thoughtful and constructive comments, which are much appreciated.

References

Agrell, S.O. (1965) Polythermal metamorphism of limestones at Kilchoan, Ardnamurchan. *Mineralogical Magazine*, **34**, 1–15.

Armbruster, T., Yang, P. and Liebich, B.W. (1996) Mechanism of the SiO_4 for CO_3 substitution in defernite, $Ca_6(CO_3)_{1.58}(Si_2O_7)_{0.21}(OH)_7[Cl_{0.50},(OH)_{0.08}(H_2O)_{0.42}]$: a single-crystal X-ray

study at 100 K. *American Mineralogist*, **81**, 625–631.

Beard, A.D. and Drake, S.M. (2007) A melilite-bearing high-temperature calcic skarn, Camasunary Bay, Isle of Skye. *Scottish Journal of Geology*, **43**, 57–67.

Bennett, J.M., Gard, J.A., Speakman, K. and Taylor, H.F.W. (1966) $Ca_8Si_5O_{18}$ and the nature of "γ-dicalcium silicate hydrate". *Nature*, **209**, 1127.

Bolio-Arceo, H. and Glasser, F.P. (1990) Formation of spurrite, $Ca_5(SiO_4)_2CO_3$. *Cement and Concrete Research*, **20**, 301–307.

Brown, I.D. (2002) *The Chemical Bond in Inorganic Chemistry: The Bond Valence Model*. Oxford University Press, Oxford, UK, 279 pp.

Bruker (1999) *SMART and SAINT-Plus. (versions 6.01)*. Bruker AXS Inc., Madison, Wisconsin, USA.

Donskaya, T.V., Sklyarov, E.V., Gladkochub, D.P., Mazukabzov, A.M., Sal'nikova, E.B., Kovach, V.P., Yakovleva, S.Z. and Berezhnaya, H.G. (2000) The Baikal collisional metamorphic belt. *Doklady RAS*, **374**, 1075–1079, [in Russian].

Eitel, W. (1923) Über das binäre System $CaCO_3$–Ca_2SiO_4 und den Spurrit. *Neues Jahrbuch der Mineralogie, Geologie und Paläontologie, Beilageband*, **48**, 63–74.

Fedorovsky, V.S. (2004) *Geological map of south-eastern part of Ol'khon region*. The Vernadsky State Geological Museum RAS, Moscow.

Fedorovsky, V.S. and Sklyarov, E.V. (2010) The Olkhon geodynamic proving ground (lake Baikal): high resolution satellite data and geological maps of new generation. *Geodynamics & Tectonophysics*, **4**, 331–418, [in Russian].

Fedorovsky, V.S., Sklyarov, E.V., Izokh, A.E., Kotov, A.B., Lavrenchuk, A.V. and Mazukabzov, A.M. (2010) Strike-slip tectonics and subalkaline mafic magmatism in the Early Paleozoic collisional system of the western Baikal region. *Geology and Geophysics*, **51**, 682–700, [in Russian]. English version: *Russian Geology and Geophysics*, **51**, 429–442.

Galuskin, E.V., Gazeev, V.M., Lazic, B., Armbruster, T., Galuskina, I.O., Zadov, A.E., Wrzalik, R., Dzierzanowski, P., Gurbanov, A.G. and Bzowska, G. (2009) Chegemite $Ca_7(SiO_4)_3(OH)_2$ – a new humite-group calcium mineral from the Northern Caucasus, Kabardino-Balkaria, Russia. *European Journal of Mineralogy*, **21**, 1045–1059.

Galuskin, E.V., Lazic, B., Savelyeva, V.B., Armbruster, T., Galuskina, I.O., Zadov, A.E., Dzierżanowski, P., Pertsev, N.N. and Gazeev, V.M. (2011) Pavlovskyite, IMA 2010-063. CNMNC Newsletter No. 8, April 2011, page 290; *Mineralogical Magazine*, **75**, 289–294.

Galuskina, I.O., Lazic, B., Armbruster, T., Galuskin, E.V., Gazeev, V.M., Zadov, A.E., Pertsev, N.N., Jezal, L., Wrzalik, R. and Gurbanov, A.G. (2009) Kumtyubeite $Ca_5(SiO_4)_2F_2$ – a new calcium mineral of the humite group from Northern Caucasus, Kabardino-Balkaria, Russia. *American Mineralogist*, **94**, 1361–1370.

Glasser, F.P. (1973) The formation and thermal stability of spurrite, $Ca_5(SiO_4)_2CO_3$. *Cement and Concrete Research*, **3**, 23–28.

Garbev, K. (2004) *Struktur, Eigenschaften und quantitative Rietveldanalyse von hydrothermal kristallisierten Calciumsilikathydraten (C-S-H-Phasen)*. Scientific report of the Karlsruhe Research Centre, FZKA 6877, Karlsruhe, Germany, 241 pp.

Garbev, K., Gasharova, B., Beuchle, G., Kreisz, S. and Stemmermannn, P. (2008) First observation of α-$Ca_2[SiO_3(OH)](OH)$–$Ca_6[Si_2O_7][SiO_4](OH)_2$ phase transformation upon thermal treatment in air. *Journal of the American Ceramic Society*, **91**, 263–271.

Grice, J.D. (2005) The structure of spurrite, tilleyite and scawtite, and relationships to other silicate-carbonate minerals. *The Canadian Mineralogist*, **43**, 1489–1500.

Hawthorne, F.C. and Schindler, M. (2008) Understanding the weakly bonded constituents in oxysalt minerals. *Zeitschrift für Kristallographie*, **223**, 41–68.

Henmi, C. and Henmi, K. (1978) Synthesis of spurrite and tilleyite at low CO_2 partial pressure. *Mineralogical Journal*, **9**, 106–110.

Henmi, C., Kusachi, I., Kawahara, A. and Henmi, K. (1977) Fukalite, a new calcium carbonate silicate hydrate mineral. *Mineralogical Journal*, **8**, 374–381.

Joesten, R. (1976) High-temperature contact metamorphism of carbonate rocks in a shallow crustal environment, Christmas Mountains, Big Bend region, Texas. *American Mineralogist*, **61**, 776–781.

Jost, K.H., Ziemer, B. and Seydel, R. (1977) Redetermination of the structure of β-dicalcium silicate. *Acta Crystallographica*, **B33**, 1696–1700.

Kapralik, I., Stevula, L., Petrovic, J. and Hanic, F. (1984) Study of the system CaO–SiO_2–CO_2–H_2O in relation to scawtite under hydrothermal conditions. *Cement and Concrete Research*, **14**, 866–872.

Korikovsky, S.P. and Fedorovsky, V.S. (1981) Petrology of metamorphic rocks of the Ol'khon Region. Geology of granulites. Pp. 70–80 in: *Field trip guide of the Baikal excursion of the international symposium, Irkutsk* (F.A. Letnikov, editor). [in Russian].

Marincea, S., Bilal, E., Verkaeren, J., Pascal, M.L. and Fonteilles, M. (2001) Superposed parageneses in the spurrite-, tilleyite-, and gehlenite-bearing skarns from Cornet Hill, Apuseni Mountains, Romania. *The Canadian Mineralogist*, **39**, 1435–1453.

Mekhonoshin, A.S., Vladimirov, A.G., Fedorovsky, V.S., Volkova, N.I., Travin, A.V., Kolotilina, T.B., Khromych, S.V. and Yudin, D.S. (2004) Mafic-ultramafic magmatism of the Ol'khon collisional system (West Baikal Area): $^{40}Ar/^{39}Ar$ age and structural position. Geodynamic evolution of the lithosphere of the Central-Asian foldbelt (from ocean to continent). Pp. 40–43 in: *Proceedings of Scientific Conference in the Frame of Fundamental Research*. IG SO RAS publishing, Irkutsk, Russia, [in Russian].

Merlino, S., Bonaccorsi, E, Grabezhev, A.I., Zadov, A.E., Pertsev, N. N. and Chukanov, N.V. (2009) Fukalite: an example of an OD structure with two-dimensional disorder. *American Mineralogist*, **94**, 323–333.

Novoselova, M.R. and Turutanov, E.Kh. (1982) Morphology of Ozersky and Krestovsky gabbroid massifs of the Baikal region. *Soviet Geology*, **5**, 111–116, [in Russian].

Sarp, H., Taner, M.F., Deferne, J., Bizouard, H. and Liebich, B.W. (1980) La defernite, $Ca_6(CO_3)_2(OH,Cl)_8.nH_2O$, un nouveau carbonate de calcium chloro-hydroxylé. *Bulletin de Minéralogie*, **103**, 185–189, [in French].

Savelyeva, V.B., Uschapovskaya, Z.P. and Nartova, N.V. (1992) On the kilchoanite rock at Priol'khonye (west Baikal region). *Zapiski Rossiiskogo Mineralogicheskogo Obshchestva*, **121**, 111–117.

Sheldrick, G.M. (1996) *SADABS*. University of Göttingen, Germany.

Sheldrick, G.M. (2008) A short history of *SHELX*. *Acta Crystallographica*, **A64**, 112–122.

Shimazaki H., Miyawaki, R., Yokoyama, K., Matsubara, S. and Bunno, M. (2008) Occurrence and new data of dellaite from the Akagane mine, Japan. *Journal of Mineralogical and Petrological Sciences*, **103**, 385–389.

Sokol, E.V., Novikov, I.S., Zateeva, S.N, Sharygin, V.V. and Yapnik, Y. (2008) Pyrometamorphic rocks of the spurrite-merwinite facies as indicators of hydrocarbon discharge zones (the Hatrurim formation, Israel). *Doklady Earth Sciences*, **420**, 608–614.

Speakman, K., Taylor, H.F.W., Bennett, J.M. and Gard, J.A. (1967) Hydrothermal reactions of γ-dicalcium silicate. *Journal of the Chemical Society A: Inorganic, Physical, Theoretical*, **1967**, 1052–1060.

Taylor, H.F.W. (1997) *Cement Chemistry*. Thomas Telford, London, 459 pp.

Tilley, C.E. (1929) On larnite (calcium orthosilicate, a new mineral) and its associated minerals from the limestone contact-zone of Scawt Hill, Co. Antrim. *Mineralogical Magazine*, **22**, 77–86.

Tilley, C.E. and Hey, M.H. (1930) Scawtite, a new mineral from Scawt Hill, Co. Antrim. *Mineralogical Magazine*, **22**, 222–224.

Treiman, A.H. and Essene, E. (1983) Phase equilibria in the system $CaO–SiO_2–CO_2$. *American Journal of Science*, **283A**, 97–120.

Tuttle, O.F. and Harker, R.I. (1957) Synthesis of spurrite and the reaction wollastonite + calcite = spurrite + carbon dioxide. *American Journal of Science*, **255**, 226–234.

Vladimirov, V.G., Korneva, I.B., Semenov, I.V. and Yudin, D.S. (2009) Structural-kinematic position of the Birkhin massif as indicator of the Ol'khon region evolution (eastern Baikal region). Geodynamic evolution of lithosphere of Asian mobile belt (from ocean to continent). Pp. 62–64 in: *Proceedings of Scientific Conference in the Frame of Fundamental Research*. IG SO RAS publishing, Irkutsk, Russia, [in Russian].

Wright, F.E. (1908) On three contact minerals from Velardena, Durango, Mexico (gehlenite, spurrite and hillebrandite). *American Journal of Science*, **26**, 545–554.

Wyllie, P.J. and Haas, J.L. (1965) The system $CaO–SiO_2–CO_2–H_2O$: I. Melting relationships with excess vapor at 1 kilobar pressure. *Geochimica et Cosmochimica Acta*, **29**, 871–892.

Wyllie, P.J. and Haas, J.L. (1966) The system $CaO–SiO_2–CO_2–H_2O$: II. The petrogenetic model. *Geochimica et Cosmochimica Acta*, **30**, 525–543.

Yvon, K., Jeitschko, W. and Parthé, E. (1977) *LAZY PULVERIX*, a computer program, for calculating X-ray and neutron diffraction powder patterns. *Journal of Applied Crystallography*, **10**, 73–74.

Zharikov, V.A. and Shmulovich, K.I. (1969) High-temperature mineral equilibrium in the system $CaO–SiO_2–CO_2$. *Geochemistry*, **9**, 1039–1056, [in Russian].